Parametric Sensitivity in a Generalized Model for Atmospheric Pressure Chemical Ionization Reactions

Lattouf, Elie

2021-08-04

Lattouf , E , Anttalainen , O A , Kotiaho , T , Hakulinen , H I , Vanninen , P & Eiceman , G A 2021 , ' Parametric Sensitivity in a Generalized Model for Atmospheric Pressure Chemical Ionization Reactions ' , Journal of the American Society for Mass Spectrometry , vol. 32 , no. þÿ 8 , pp. 2218 2226 . https://doi.org/10.1021/jasms.1c00158

http://hdl.handle.net/10138/334409
https://doi.org/10.1021/jasms.1c00158

ACS Partner Journal

Journal of the American Society for Mass Spectrometry

pubs.acs.org/jasms

Research Article

Parametric Sensitivity in a Generalized Model for Atmospheric Pressure Chemical Ionization Reactions

Elie Lattouf,* Osmo Anttalainen, Tapio Kotiaho, Hanna Hakulinen, Paula Vanninen, and Gary Eiceman

Cite This: *J. Am. Soc. Mass Spectrom.* 2021, 32, 2218−2226

Read Online

ACCESS | Metrics & More | Article Recommendations | Supporting Information

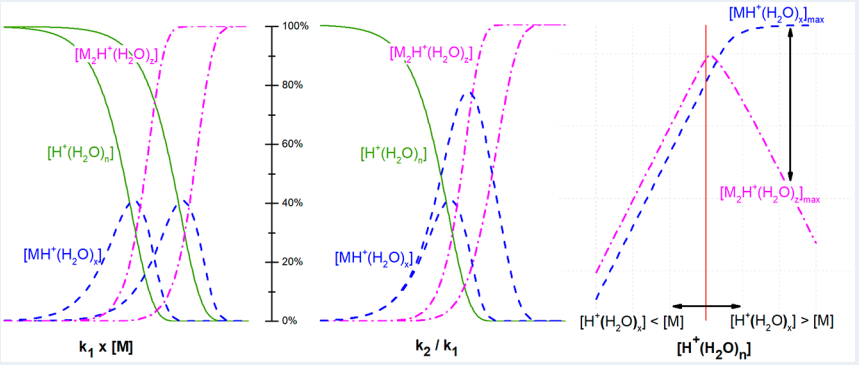

ABSTRACT: Gas phase reactions between hydrated protons $H^+(H_2O)_n$ and a substance M, as seen in atmospheric pressure chemical ionization (APCI) with mass spectrometry (MS) and ion mobility spectrometry (IMS), were modeled computationally using initial amounts of [M] and $[H^+(H_2O)_n]$, rate constants k_1 to form protonated monomer $(MH^+(H_2O)_x)$ and k_2 to form proton bound dimer $(M_2H^+(H_2O)_z)$, and diffusion constants. At 1×10^{10} cm^{-3} (0.4 ppb) for $[H^+(H_2O)_n]$ and vapor concentrations for M from 10 ppb to 10 ppm, a maximum signal was reached at 4.5 μs to 4.6 ms for $MH^+(H_2O)_x$ and 7.8 μs to 46 ms for $M_2H^+(H_2O)_z$. Maximum yield for protonated monomer for a reaction time of 1 ms was ~40% for k_1 from 10^{-11} to 10^{-8} $cm^3 \cdot s^{-1}$, for $k_2/k_1 = 0.8$, and specific values of [M]. This model demonstrates that ion distributions could be shifted from $[M_2H^+(H_2O)_z]$ to $[MH^+(H_2O)_x]$ using excessive levels of $[H^+(H_2O)_n]$, even for [M] > 10 ppb, as commonly found in APCI MS and IMS measurements. Ion losses by collisions on surfaces were insignificant with losses of <0.5% for protonated monomer and <0.1% for proton bound dimer of dimethyl methylphosphonate (DMMP) at 5 ms. In this model, ion production in an APCI environment is treated over ranges of parameters important in mass spectrometric measurements. The models establish a foundation for detailed computations on response with mixtures of neutral substances.

KEYWORDS: *atmospheric pressure chemical ionization, reaction kinetics, hydrated proton, rate constant, vapor concentration, protonated monomer, proton bound dimer*

INTRODUCTION

Analytical response in atmospheric pressure chemical ionization (APCI) mass spectrometry (MS)[1−4] and ion mobility spectrometry (IMS) at ambient pressure[5,6] is governed by gas phase reactions between analyte neutrals and reagent ions, often derived from proton clusters in positive polarity. Such reactions occur in a significant number of ion sources for MS[7,8] including corona discharges,[9,10] electrospray ionization,[11−13] dielectric barrier discharges,[14,15] and soft X-rays.[16−18] One stable and reliable source at ambient pressure, the beta emitter ^{63}Ni, was used in early API MS instruments[1] and can be found in IMS drift tubes in use today.[19,20] The foundations for understanding gas phase ion−molecule reactions were developed and refined by the mid-1970s[21] with a broad experimental record for mass spectrometry including chemical ionization MS[22−24] and studies with ionization detectors.[25−28] These reactions as shown in eq 1 for reactions between hydrated protons (reagent) and substances M (analyte) commonly occur at elevated or ambient pressure with ions at thermal energies. Favorable interactions between M and $H^+(H_2O)_n$ form an energetic intermediate $(MH^+(H_2O)_n)^*$ which undergoes loss of neutrals to form a protonated monomer, $MH^+(H_2O)_x$:

$$\underset{\text{hydrated proton/ reactant or reagent ion}}{H^+(H_2O)_n} + \underset{\text{analyte}}{M} \leftrightarrow \underset{\text{protonated monomer}}{MH^+(H_2O)_x} + \underset{\text{neutral}}{yH_2O} \quad (1)$$

Received: May 10, 2021
Revised: June 22, 2021
Accepted: June 23, 2021
Published: July 15, 2021

Residence times and collision frequencies are often sufficient to result in larger cluster ions such as proton bound dimers shown in eq 2.

$$\underset{\text{protonated monomer}}{MH^+(H_2O)_x} + \underset{\text{analyte}}{M} \leftrightarrow \underset{\text{proton bound dimer}}{M_2H^+(H_2O)_z} + \underset{\text{neutral}}{wH_2O} \quad (2)$$

While proton bound trimers can form at subambient temperatures and are observed in mobility spectra, ion lifetimes are submillisecond at or above 25 °C and are not commonly seen in applications of IMS today with 1 to 10 ms time scale.[29,30] Only reactions with hydrated protons are considered in models developed here although recent studies have demonstrated that precursor ions including O_2^+ can be utilized at high electric fields and reduced pressures.[31]

In more a generalized expression, the waters of hydration in eq 1 can be replaced by solvent molecules or other substance such as acetone or ammonia to control or enhance selectivity of response in some IMS and MS measurements.[5,6,32,33] Details on reaction enthalpies, mechanisms, and influences of ion structures were extensively explored from ∼1965 to 1990 for reactions in eqs 1 and 2 with ion sources at high or ambient pressure.[34−43] Interest was given particularly to refined models of the Langevin rate constant[44] and detailed descriptions of bimolecular collisions.[45] Significantly, only a limited experimental record, obtained largely at subambient pressures using selected ion flow tube mass spectrometry, exists on rate constants specifically for hydrated protons, and these studies were from Kebarle et al.,[38] Bohme et al.,[42,43] Castleman et al.,[46,47] and others[48,49] are also relevant. Rate constants for formation of proton bound dimers are known only from studies with ion mobility spectrometry.[50]

Insights into reaction kinetics have been used in several APCI reaction studies where models were developed to predict or interpret responses in APCI MS or IMS, and these studies were largely targeted to specific designs of technology or substances.[51−53] In a model of response with reactions in a cylindrical source as found in early APCI MS designs, Siegel described ion density of positive and negative ions formed from a beta emitter.[54] A thorough discussion was given to the production of ions and their losses from recombination and diffusion with an emphasis on source parameters and design. This model was adapted and extended by Ketkar et al. and compared to analytical response in APCI MS with a corona discharge ion source.[55] The change in response to dimethyl methylphosphonate (DMMP) in the presence of a second constituent, diisopropyl methylphosphonate (DIMP), was determined experimentally and compared favorably with predicted values for reaction times of 0.1 ms. Recently, response of an ion mobility spectrometer to DMMP was compared to models derived from the work of Siegel and included the formation of proton bound dimer with reaction times of 10−100 μs.[53,56] Predicted and measured ion abundances were comparable until reaction times >100 μs after which divergence occurred and was attributed to recombination reactions. Other models for glow discharge sources in mass spectrometry[57] and for proton transfer reaction mass spectrometry[44] are noteworthy yet limited for use in models here by differences in ionization chemistry.

Response using hydrated protons in an APCI MS instrument equipped with a corona discharge was quantitatively described where reaction times were established by the electric fields, gas flows, and distances between the ion source and vacuum interface.[36] High sensitivity with rate constants of 2×10^{-9} cm^3 s^{-1} were observed for nitrogenous bases where a product ion was formed on every collision between M and $H^+(H_2O)_n$. In contrast, not every collision between a hydrated proton and M forms a product ion with compounds of lesser gas phase basicity. This is seen in differing sensitivities (ion counts s^{-1} ppb^{-1}) in APCI MS which ranged from 10^2 to 10^3 for compounds with differences in gas phase basicity of 160 kJ/mol. Indeed, sensitivities for compounds with lesser gas phase basicity were increased with increased temperature.[58] Such increases can be achieved also with decreased levels of moisture as shown recently with response or sensitivity for IMS.[59,60] Finally, principles derived from reaction kinetics were used to enhance selectivity of APCI MS through extended reaction times with ultratrace vapor concentrations.[61]

Where models of APCI reactions have been provided, interests have been targeted by specific compounds, by precise applications for chemical measurements,[62] or by design considerations for ion sources[54] and models or computational tools have not been sufficiently general to explore broadly the sensitivity of reaction kinetics to various parameters. In this work, a model of APCI reactions has been developed and has been used to explore the impact of parameters on the rate of formation of protonated monomers and proton bound dimers for single substances. The goal in this work is to provide quantitative measures for APCI reactions with sufficient breath to inform the design and development of new sources for APCI MS and IMS and for analysis of response with existing sources and instrumentation.

DESCRIPTION OF MODEL

Details of Model. The model for APCI reactions is based on binary kinetics between hydrated protons and an analyte (M) in air at or near ambient pressure with certain assumptions and limitations here:

1. Reactant ions, $H^+(H_2O)_n$, are extracted from an ion source and mixed with sample vapor (M). There is no ion loss from recombination since there are no negative species in the reaction volume. The level of hydration (n) and $[H_2O]$ are assumed constant.
2. Charge density for hydrated protons is fixed at an initial value and no further addition of charge is made during the reaction time. Computations are stopped when $[H^+(H_2O)_n]$ or $[M] = 10^{-2}$ cm^{-3} for eq 1 and also when $[MH^+(H_2O)_x] = 10^{-2}$ cm^{-3} for eq 2.
3. Losses from diffusion are included for ions in a cylindrical geometry of radius r and height $(h) = 2r$.[54]
4. Moisture and temperature are "fixed" so the water cluster size n, in $H^+(H_2O)_n$, is considered to be a weighted average between ∼2.5 and 3.5, consistent with rate constants reported by Bohme et al.[63]
5. There is no loss of ion density from dilution by gas flow or extraction of ions from the reaction volume.
6. Backward reactions are considered negligible. Once formed, a product ion lifetime exceeds the time scale of any experiment. That is $k_{reverse} \ll k_{forward}$ in eqs 1 and 2.
7. Higher order ions such as proton bound trimers and tetramers are not considered due to short lifetimes.
8. Coulombic repulsions[64] are not included in this model.
9. The model is general and suitable for use with above-ambient pressure where rate constants are increased significantly with increased pressure;[65] thus, rate con-

https://doi.org/10.1021/jasms.1c00158
J. Am. Soc. Mass Spectrom. 2021, 32, 2218−2226

stants are higher than those sometimes seen in API conditions.

10. Recycling of [M] from diffusion-based neutralization of $M_2H^+(H_2O)_z$ was shown to be less than 1% for reaction times below 10 ms and was omitted.
11. The model did not include reactions between $H^+(H_2O)_n$ and 2M or M_2 since rate constants or ion lifetimes are unknown.
12. The compounds are assumed to be volatile and chemically stable with ranges of reactivities toward hydrated protons, and vapor concentrations are from sub-ppb to low ppm ranges.

Rate Equations. The rate of change in protonated monomer, or $[MH^+(H_2O)_x]$, in eq 1 is described mathematically in eq 3 and simplified without recombination since this model is based on a unipolar condition (i.e., hydrated protons have been extracted from an ion source into a reaction volume free of negative charge). The model includes loss of ion density by ion diffusion and collision on surfaces of the reaction volume. The positive term in the right side of this equation refers to the rate at which $MH^+(H_2O)_x$ ions are formed during the time interval dt, whereas the negative expressions indicates the losses by sequential reactions, i.e. formation of proton bound dimer, or $M_2H^+(H_2O)_z$, and diffusion losses. Here, k_1 is the reaction rate constant of the reaction, [M] is the abundance of the neutral compound, D_+ is the diffusion constant for positive ions over the diffusion length Λ.

$$\frac{d[MH^+(H_2O)_x]}{dt} = k_1[M][H^+(H_2O)_n] - k_2[M][MH^+(H_2O)_x] - \frac{D_+}{\Lambda^2}[MH^+(H_2O)_x] \quad (3)$$

$$\frac{d[M_2H^+(H_2O)_z]}{dt} = k_2[M][MH^+(H_2O)_x] - \frac{D_+}{\Lambda^2}[M_2H^+(H_2O)_z] \quad (4)$$

$$\frac{d[H^+(H_2O)_n]}{dt} = -k_1[M][H^+(H_2O)_n] - \frac{D_+}{\Lambda^2}[H^+(H_2O)_n] \quad (5)$$

$$\frac{d[M]}{dt} = -k_1[M][H^+(H_2O)_n] - k_2[M][MH^+(H_2O)_x] \quad (6)$$

Units in the computations differ from SI units in time and volume to match the familiar literature on ion molecule reaction kinetics. Time in ms or μs and volume in cm^3 also match the parameters of experimental technology.

EXPERIMENTAL SECTION

Procedures. The sensitivities of ion formation and ion distributions to reaction parameters were explored using the model described above and six experiments are described in Table 1 with lists of parameters and links to graphics. Standard parameters or initial values were drawn broadly from experiences and reports of ion−molecule reactions. Unless noted, they were the following: $[H^+(H_2O)_n] = 1 \times 10^{10}$ cm^{-3} (0.4 ppb); $k_1 = 1.0 \times 10^{-9}$ cm^3 s^{-1}; $k_2 = 0.8k_1$;[53] $D = 0.05$ cm^2 s^{-1},[54] $r = 1.5$ cm; $h = 2r$, and [M] = 10 ppb (2.46×10^{11} cm^{-3}). Reaction time is variable unless noted.

Experiment I.

Table 1. Computational Experiments Using a Model for Formation of Product Ions from Sample Neutral M and Hydrated Protons[a]

no.	name	variable and range	Figure
I	A. depletion of hydrated proton and formation of product ions at fixed vapor concentrations for a single compound ($k_1 = 1 \times 10^{-9}$ cm^3·s^{-1})	time 0−100 ms; $k_2 = 0.8k_1$	1
	B. rate of formation of protonated monomer with the formation of proton bound dimer, for a single compound, over a range of vapor concentrations [M]	time 0−2 ms; $k_2 = 0$; [M] from 2.46×10^{11} (10 ppb) to 1.23×10^{14} cm^{-3} (5000 ppb)	S1
		time 0−20 ms; [M] from 2.46×10^9 (0.1 ppb) to 2.46×10^{13} cm^{-3} (1 ppm)	2
	C. rate of formation of protonated monomer and proton bound dimer over a range vapor concentrations and for a single compound	time 0−1000 ms; [M] interval from 2.46×10^9 (0.1 ppb) to 2.46×10^{13} cm^{-3} (1 ppm)	3
II	influence of rate constant k_1 (a variety of vapor compounds) on the formation of product ions	time 0−1000 ms; k_1 interval from 1.0×10^{-11} to 1.0×10^{-8} cm^3·s^{-1}	4
III	influence of k_1[M] on the formation of product ions	time = 1 ms; k_1 from 1.0×10^{-11} to 1.0×10^{-8} cm^3·s^{-1}; [M] interval from 0.1 to 10000 ppb (0.0001 to 10 ppm)	5
IV	A. influence of the dimerization rate constant k_2 on the relative ion yield of product ions	time = 1 ms; k_2/k_1 0.1, 0.5, and 0.8	6
	B. influence of k_2 on the formation of product ions	time 0−1000 ms; k_2/k_1 interval from 0 to 0.9	7
	C. influence of k_2 on the maximum protonated monomer yield, for various rate constants k_1 over an interval of k_2	time (t) variable, at time of $[MH^+(H_2O)_x]_{max}$, $[MH^+(H_2O)_x]_{max}$, and $[M_2H^+(H_2O)_z]_{max}$ refers to the maximum yield of product ions obtained across all reaction times; $[H^+(H_2O)_n]$ 1×10^{10} cm^{-3}; k_1 from 1.0×10^{-11} to 5.0×10^{-9} cm^3·s^{-1}; k_2/k_1 interval from 0 to 0.9	S2
V	effects of $[H^+(H_2O)_n]$ on relative product ions yield—limiting reagent	time (t) variable, at time of maximum yield ($[M]_{reacted}/[M]_{initial}$) × 100; $[H^+(H_2O)_n]$ 1×10^7 to 1×10^{13} cm^{-3}; [M] 0.1, 1, 10, and 100 ppb	8
VI	impact on ion density from losses of ions by diffusion and collision on walls of reaction volume for DMMP	time 0−100 ms; rate constants[53] $k_1 = 1.35 \times 10^{-9}$ cm^3·s^{-1}, $k_2 = 1.09 \times 10^{-9}$ cm^3·s^{-1}; diffusion constants D for $[H^+(H_2O)_n]$ 0.056 cm^2·s^{-1}, for $MH^+(H_2O)_x$ 0.049 cm^2·s^{-1}, for $M_2H^+(H_2O)_z$ 0.037 cm^2·s^{-1}	S3

[a]The model was based on standard parameters (see text) unless noted.

https://doi.org/10.1021/jasms.1c00158
J. Am. Soc. Mass Spectrom. 2021, 32, 2218−2226

A. The depletion of $[H^+(H_2O)_n]$ and the formation of product ions $MH^+(H_2O)_x$ and $M_2H^+(H_2O)_z$, for a single compound reacting with a fixed k_1. Standard parameters were used with the model for a time step <1 μs from 0 to 100 ms. Plots were made in OriginLab for ion densities with time.

   Only the formation of $MH^+(H_2O)_x$ occurs: in this experiment, the sequential reaction to $M_2H^+(H_2O)_z$ was not included in the model ($k_2 = 0$ in eqs 3, 4, and 6) to show behavior for substances that do not form proton bound dimers. Standard parameters were used with a broad range of vapor concentrations for times from 0 to 2 ms.

B. The formation of $MH^+(H_2O)_x$ and $M_2H^+(H_2O)_z$ for a specific substance ($k_1 = 1 \times 10^{-9}$ cm^3 s^{-1}). In this experiment, the sequential reaction to $M_2H^+(H_2O)_z$ was included in the model ($k_2 = 0.8k_1$) in eqs 3, 4, and 6. Five values for vapor concentration were considered: 0.1, 1, 10, 100, and 1000 ppb and plots for ion yield are shown as a function of time.

C. The formation of product ions over an interval of vapor concentrations and time.

Experiment II. The formation of product ions over an interval of rate constants k_1 as a function time.

Experiment III. Four values of k_1 extracted from experiment II-C for line plots of ion yield at 1 ms, as a function of an interval of [M].

Experiment IV.

A. The rate of formation of $MH^+(H_2O)_xM_2H^+(H_2O)_z$ over a range of ratios for k_2/k_1 of 0.1, 0.5, and 0.8 for a fixed reaction time of 1 ms and an interval of [M].

B. The rate of formation of $MH^+(H_2O)_x$ and $M_2H^+(H_2O)_z$ over an interval of k_2/k_1 ratios.

C. The monomer $MH^+(H_2O)_x$ maximum yield as a function of an interval of k_2 for various compounds (i.e., k_1).

Experiment V. Influence of the reactant ion $[H^+(H_2O)_n]$ on product ion yield and the effect of the limiting reagent on the distribution of $[MH^+(H_2O)_x]$ and $[M_2H^+(H_2O)_z]$.

Experiment VI. The density of each ion species decreased by diffusion and collision on walls of the reaction volume. Loss of charge upon collision with a surface was modeled for dimethyl methylphosphonate (DMMP).

Computational Procedures. *MatLab.* The system of differential equations (eqs 3−6) was introduced into MatLab R2021a from MathWorks in order to find instantaneous analytic solutions. The latter were found from nested "for loops", for time and another varying parameter (i.e., k_1, k_2, [M]; see Table 1). For each value of the latter, the equations were solved for the entire time interval with a step size Δt, filling output arrays with instantaneous values. The time step size Δt was chosen carefully (i.e., $\Delta t \ll 1/k_1[M]$) so that concentrations are not depleted rapidly in a few iterations, implicating unresolved solutions. Limiting reagents were taken into consideration: when one of the reactants is depleted, its consumption stops and so does the reaction. Only a limited number of elements was selected in time, as a sample from the output matrices of interest and exported in text files, to avoid graphics memory saturation when plotting contour plots. The reduced matrices were imported into OriginPro 2020 SR1 9.7.0.188, from OriginLab Corp. for plotting. MatLab files are accessible under the open access documentation (European Union's Horizon 2020 FET Open program under grant agreement no. 899261) at https://www.jottacloud.com/s/2616d6f1a4adba34e928097bc2be3e3e3f2.

RESULTS AND DISCUSSION

Vapor Concentration and Ion Distributions. The abundances of protonated monomer and proton bound dimer with a single neutral substance (M) at a vapor concentration of 2.46×10^{11} cm^{-3} (or 10 ppb) are shown in Figure 1 for reaction

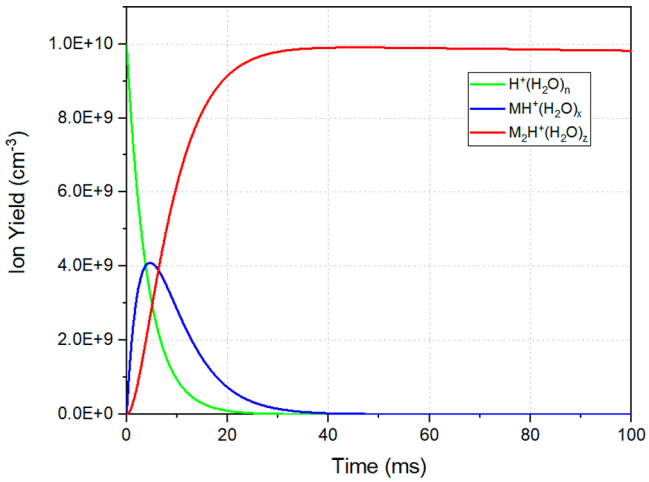

Figure 1. Time-dependent changes in ion densities for reaction of M with $H^+(H_2O)_n$ for [M] = 10 ppb (= 2.46×10^{11} cm^{-3}).

times of 0−100 ms (experiment IA, Table 1). The plot for ion density of $H^+(H_2O)_n$ follows eq 5 and is consistent with second order kinetics. The stepwise formation of product ions through eqs 1 and 2 can be seen in the increase in $[MH^+(H_2O)_x]$ from t = 0−4.5 ms and in the increase in $[M_2H^+(H_2O)_z]$ with concurrent decrease in $[MH^+(H_2O)_x]$. The sequential nature of this reaction is seen also in the growth in intensity for $MH^+(H_2O)_x$ and the slight lag by a few milliseconds in the appearance and an increase in intensity for $M_2H^+(H_2O)_z$.

After this time, $[M_2H^+(H_2O)_z]$ continues to increase until $[MH^+(H_2O)_x]$ is depleted at ~45 ms as $[H^+(H_2O)_n]$ is depleted at ~30 ms. Since $[H^+(H_2O)_n]$ was initially 1×10^{10} cm^{-3} (~0.4 ppb), there is an excess density of 2.26×10^{11} cm^{-3} for M) when the reaction has proceed entirely to $[M_2H^+(H_2O)_z]$; this constitutes a reaction yield for M of only 8.11%. A gradual decrease in $[M_2H^+(H_2O)_z]$ between 40 to 60 ms arises from ion diffusion and collisions on surfaces of the reaction volume under quiescent flow condition exclusive of Coulombic repulsions.[64,66]

Reaction times to reach maximum $[MH^+(H_2O)_x]$ were dependent on the concentration of M and some representative values were the following: 45.3 μs for 2.46×10^{13} cm^{-3} (1000 ppb); 90.6 μs for 1.23×10^{13} cm^{-3} (500 ppb); 454 μs for 2.46×10^{12} cm^{-3} (100 ppb); 909 μs for 1.23×10^{12} cm^{-3} (50 ppb); and 4.62 ms for 2.46×10^{11} cm^{-3} (10 ppb) (see Table 2). This dependence is also shown partially in Figure 2 for reaction times under 20 ms.

Where reactions form proton bound dimers, reaction times to full response or maximum $[M_2H^+(H_2O)_z]$ are shown in Table 2 and seen in Figure 2 (dashed lines). They could reach times of 45.63 ms for [M] = 10 ppb, also with unreacted M, e.g., 91.89% excess at 10 ppb to 99.99% excess 10 ppm (Table 2). A complete description for ion distributions, reaction times, and vapor concentrations is shown as a contour plot in Figure 3 and encompasses parameters of modern APCI MS and IMS

https://doi.org/10.1021/jasms.1c00158
J. Am. Soc. Mass Spectrom. 2021, 32, 2218−2226

Table 2. Metrics for Reaction of M with $H^+(H_2O)_n$ Leading to Formation of $MH^+(H_2O)_x$ and $M_2H^+(H_2O)_z$[a]

[M] ppm	$[MH^+(H_2O)_x]$ cm^{-3} ($\times 10^9$)	$[MH^+(H_2O)_x]_{max}/[H^+(H_2O)_n]_{initial}$	time to $[MH^+(H_2O)_x]_{max}$ ms	$[M_2H^+(H_2O)_z]$ cm^{-3} ($\times 10^9$)	$[M_2H^+(H_2O)_z]_{max}/[H^+(H_2O)_n]_{initial}$	time to $[M_2H^+(H_2O)_z]_{max}$ ms	unreacted [M] cm^{-3} ($\times 10^{14}$)	% unreacted M
0.01	4.0925	0.40925	4.6183	9.9064	0.99064	45.627	0.0022643	91.892
0.05	4.0953	0.40953	0.90913	9.9790	0.99790	10.394	0.012120	98.375
0.1	4.0957	0.40957	0.45368	9.9889	0.99889	5.5257	0.024441	99.187
0.5	4.0962	0.40962	0.090590	9.9975	0.99975	1.2654	0.12300	99.836
1	4.0964	0.40964	0.045280	9.9987	0.99987	0.66782	0.24621	99.917
5	4.0983	0.40982	0.0090500	9.9997	0.99997	0.14990	1.2318	99.982
10	4.1005	0.41005	0.0045200	9.9999	0.99998	0.078440	2.4639	99.990

[a]Values for [M] in cm^{-3} are shown in Table 3. Comments on significant figures are found in Supporting Information.

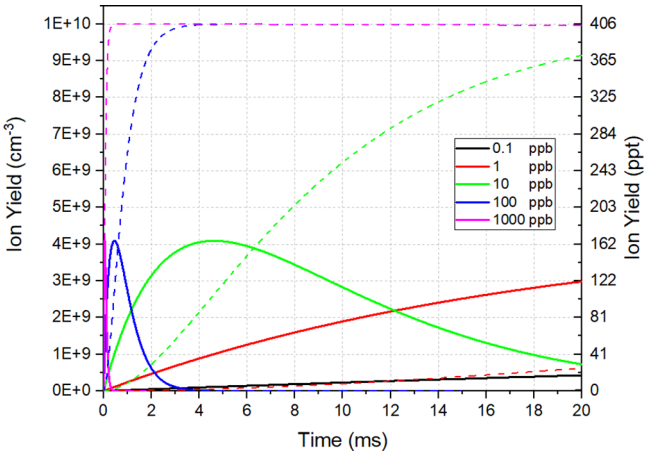

Figure 2. Time-dependent changes for $[MH^+(H_2O)_x]$ (solid lines) and $[M_2H^+(H_2O)_z]$ (dashed lines), at five vapor concentrations of M.

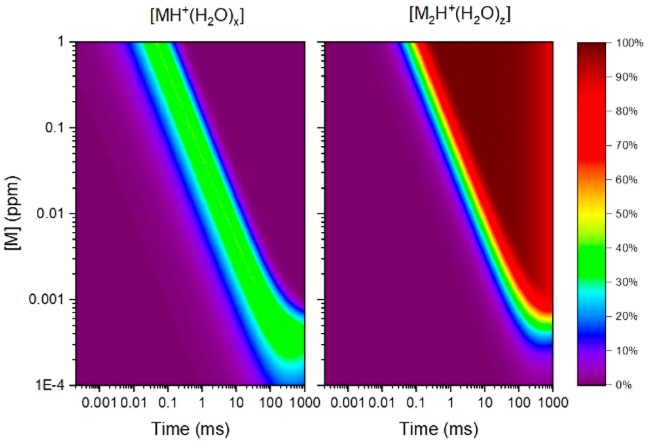

Figure 3. Contour plots of $[MH^+(H_2O)_x)]$ and $[M_2H^+(H_2O)_z)]$ in percent of initial $[H^+(H_2O)_n]$, vapor concentration, and reaction time under standard conditions of the model.

measurements. The plots show that reaction times for maximum yield of $MH^+(H_2O)_x$ are dependent on vapor concentration and that $MH^+(H_2O)_x$ is depleted by $M_2H^+(H_2O)_z$ uniformly across all [M], except at 100 to 300 ppt, where M is the limiting reagent. In this region, the limiting reagent is M and only $H^+(H_2O)_n$ and $MH^+(H_2O)_x$ are visible at this scaling. The protonated monomer reaches maximum ion density at times from 0.1 to >100 ms for [M] from 1 ppm to 0.1 ppb, respectively.

The scale for reaction yield shows that a maximum near 40% (in percent of initial $[H^+(H_2O)_n]$, Figures 2 and 3) for $MH^+(H_2O)_x$ is reached (referenced to initial $[H^+(H_2O)_n]$), regardless of vapor concentration and reaction time.

In summary, reaction time scales for vapor concentrations of analytes, as found in IMS and API MS studies with low ppb to low ppm, occur at times from low microseconds to tens of milliseconds and are governed significantly by the onward reaction to form protonated monomers by k_1 and proton bound dimers by k_2. In the discussion above, k_1 was fixed at a relatively high value as found with compounds with favorable response such as amines or organophosphorus compounds and k_2 was fixed against k_1.[67] Differences in rate constants should also influence reaction kinetics both in time scales and in the quantitative abundances of ions.

Rates Constants and Ion Distributions. The favorability of reaction chemistry with hydrated protons is based on the strength of the dipole−ion association of M···H^+ and is described by reaction enthalpies. In reaction rates, the differences in "reactivity" are reflected in the magnitude of rate constants and these can range from 1×10^{-11} cm^3 s^{-1} for weakly reactive substances such as alkenes to $\sim 7 \times 10^{-9}$ cm^3 s^{-1} for strongly reactive substances such as amines. The influence of k_1 is shown in Figure 4 as contour plots for reaction yield, k_1, and

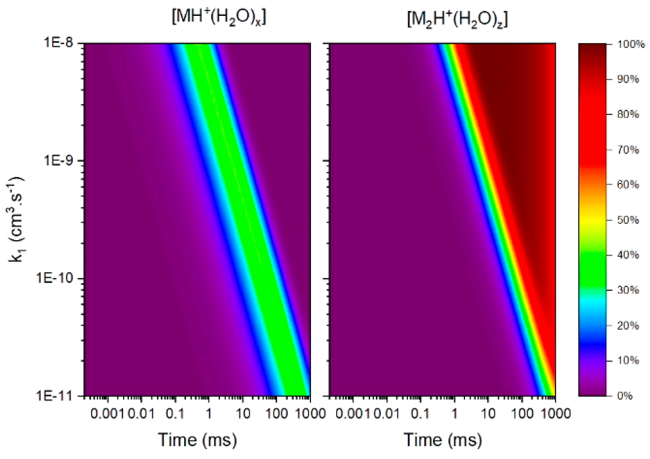

Figure 4. Contour plots of $MH^+(H_2O)_x$ and $M_2H^+(H_2O)_z$ abundances (in percent), rate constant k_1, and time under standard conditions of the model.

reaction time. Calculations show the impact of k_1 in the time to depletion of $H^+(H_2O)_n$. This occurs at 1 ms reaction time at 20 ppb for a "reactive" compound with k_1 of 1×10^{-8} cm^3 s^{-1} and in contrast will occur at 2 ppm for an "unreactive" compound with k_1 of 1×10^{-10} cm^3 s^{-1} (Figure 5).

The results are consistent with $k_1[M][H^+(H_2O)_n]$ through eq 3. At fixed reaction times (1 ms in Figure 5), the maximum

https://doi.org/10.1021/jasms.1c00158
J. Am. Soc. Mass Spectrom. 2021, 32, 2218−2226

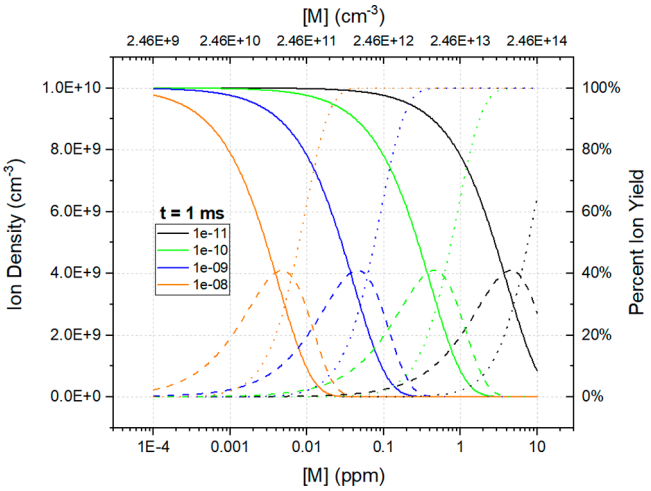

Figure 5. Sensitivity of ion abundances to $k_1 \times [M]$ at $t = 1$ ms. Plots are shown for four values of k_1 (color code in legend): (solid lines) $[H^+(H_2O)_n]$; (dashed lines) $[MH^+(H_2O)_x]$; (dotted lines) $[M_2H^+(H_2O)_z]$.

percent yield for $MH^+(H_2O)_x$ is ~40% from the product of $k_1\backslash[M]$ over a range of [M] and values for k_1. An increase in [M] would shift the maximum yield for $MH^+(H_2O)_x$ toward reaction times <1 ms (and vice versa) (Figure 3). This explains the drop in the protonated monomer yield at 1 ms for increasing [M].

Results in Figure 4 and 5 show quantitatively that maximum yield of protonated monomer spans a range of $k_1[M]$ and reaction times, although k_2 is also expected control product ion distributions.

In Figure 6, distributions of $[MH^+(H_2O)_x]_{max}$ and $[M_2H^+(H_2O)_z]_{max}$ are shown for 1 ms reaction time, over a

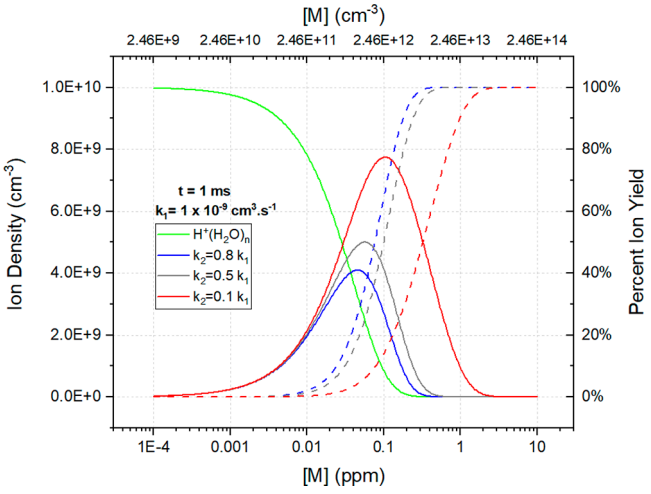

Figure 6. Sensitivity of ion abundances to k_2/k_1 (color code in legend): (solid lines) $[H^+(H_2O)_n]$ and $[MH^+(H_2O)_x]$; (dashed lines) $[M_2H^+(H_2O)_z]$.

range of [M] and ratio of k_2/k_1 where k_1 is fixed. The maximum yield for the protonated monomer, $[MH^+(H_2O)_x]_{max}$, is dependent on k_2 with characteristic values for [M] and reaches near 80% of $[H^+(H_2O)_n]_{initial}$ when k_2 is $0.1k_1$.

In Figure 7, these behaviors are shown for [M] at 10 ppb with an increased range in the ratio k_2/k_1. The protonated monomer rises, for k_2/k_1 = 0.8, above 20% from ~1 to 20 ms with a

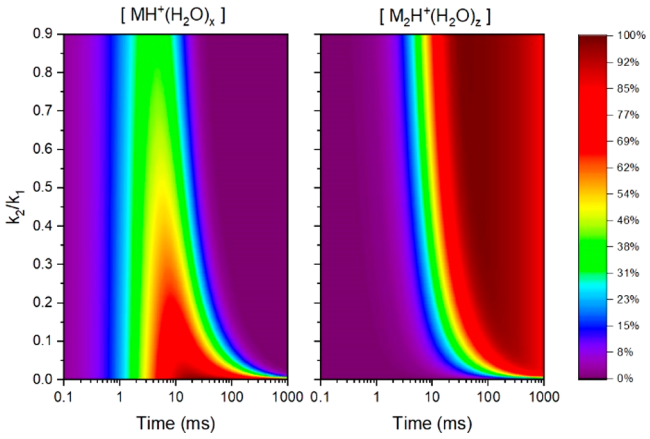

Figure 7. Contour plots of $[MH^+(H_2O)_x]$ and $[M_2H^+(H_2O)_z]$ (in percent), ratio k_2/k_1, and reaction time, at standard conditions of the model.

maximum yield ~40% near 4 ms. The maximum yield of ~20% (at 1 ms) is clearly seen in Figure 6 (blue dashed line at 10 ppb).

In contrast, a timespan of 1 ms to nearly 80 ms was obtained for $k_2/k_1 = 0.1$, where $[MH^+(H_2O)_x] > 20\%$. This ratio would be characteristic of substances with low tendency to form a proton bound dimer. In addition, reaction yield for $[MH^+(H_2O)_x)]$ will be elevated for compounds with weak reactivity for k_2 and will exceed the 40% noted above. When formation of proton bound dimer is particularly slow, reaction yield for $[MH^+(H_2O)_x)]$ could reach more than 90% (Figure S2).

Limiting Reagent, $[H^+(H_2O)_n)]$, and Relative Product Ion Yield. In all studies described above, $[H^+(H_2O)_n)]$ was the limiting reagent where excess unreacted M ranged from 95 to 99.99% (Table 3), depending on [M] and k_1. Certain aspects of ion distributions are seemingly independent of $[H^+(H_2O)_n)]$; for example, in the regime where $H^+(H_2O)_n$ is the limiting reagent ($[H^+(H_2O)_n] < [M]$), the ratio of $[MH^+(H_2O)_x]_{max}/[M_2H^+(H_2O)_z]_{max}$ is nearly constant over the range of $[H^+(H_2O)_n]$ (Figure 8). In principle, excessive levels of $H^+(H_2O)_n$ could be introduced into the reaction volume where M becomes the limiting reagent.

In Figure 8, the effect of $[H^+(H_2O)_n)]$ is shown for time-independent maximum product ion yield, for a range of [M] with standard conditions of the model. When [M] = 0.1 ppb, $[MH^+(H_2O)_x]_{max}$ and $[M_2H^+(H_2O)_z]_{max}$ increase proportionally with increased $[H^+(H_2O)_n)]$, from 1×10^7 to 1×10^9 cm^{-3}.

At even higher levels of $[H^+(H_2O)_n)]$, $[MH^+(H_2O)_x]_{max}$ continues to increase proportionally while $[M_2H^+(H_2O)_z]_{max}$ decreases. Eventually, $[MH^+(H_2O)_x]_{max}$ cannot increase indefinitely with $[H^+(H_2O)_n)]$ and reaches a plateau at a density very close to that of [M]. The decrease of $[M_2H^+(H_2O)_z]_{max}$ arises from $k_1 > k_2$, and the rapid consumption of [M] in producing $MH^+(H_2O)_x$, thus suppresses the formation of proton bound dimer via $k_2[MH^+(H_2O)_x][M]$.

Diffusion Losses. Ion density for proton bound dimers in Figures 3, 4, and 7 all exhibit a noticeable loss with reaction times >200 ms, exhibited by the fading of the red color. This loss occurs through ion collisions on walls of the reaction volume, resulting in neutralization and decreases in $[M_2H^+(H_2O)_z]$. Findings from experiment VI are shown in Figure S3 where radii of reaction volumes were 0.5−2 cm[54] and height was 2r. Under these conditions, diffusion losses for DMMP increase with decreasing volume (radii) and are below 1% for time intervals <5 ms, even for the smallest selected radius (r = 0.5 cm). Another

https://doi.org/10.1021/jasms.1c00158
J. Am. Soc. Mass Spectrom. 2021, 32, 2218−2226

Table 3. Metrics for Reaction of M with $H^+(H_2O)_n$ Leading to Formation of $MH^+(H_2O)_x$ without Formation of Proton Bound Dimer ($k_2 = 0$)

[M] ppm	[M] cm^{-3} ($\times 10^{14}$)	$[MH^+(H_2O)_x]_{max}$ cm^{-3} ($\times 10^9$)	$[MH^+(H_2O)_x]_{max}/[H^+(H_2O)_n]_{initial}$	time to maximum yield ms	unreacted [M] cm^{-3} ($\times 10^{14}$)	% unreacted M
0.01	0.0024641	9.93721	0.99372	30.122	0.0023641	95.943
0.05	0.012321	9.98531	0.99853	7.1983	0.012220	99.187
0.1	0.024641	9.99216	0.99922	3.8702	0.024540	99.592
0.5	0.12321	9.99820	0.99982	0.90275	0.12310	99.917
1	0.24641	9.99905	0.99990	0.47934	0.24630	99.957
5	1.2321	9.99979	0.99998	0.10885	1.2319	99.990
10	2.4641	9.99989	0.99999	0.057200	2.4639	99.994

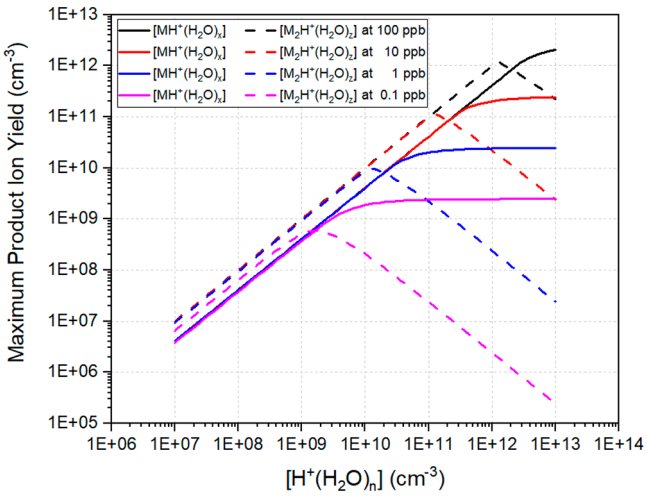

Figure 8. Influence of $[H^+(H_2O)_n]$ on maximum product ion yield for four concentrations of [M] (100 ppb = 2.46×10^{12} cm^{-3}, 10 ppb = 2.46×10^{11} cm^{-3}, 1 ppb = 2.46×10^{10} cm^{-3}, and 0.1 ppb = 2.46×10^9 cm^{-3}): (solid lines) $[MH^+(H_2O)_x]$; (dashed lines) $[M_2H^+(H_2O)_z]$.

parameter that may affect diffusion losses is the diffusion rate constant that is dependent on the ionized compound and the electric field environment. In the literature,[54] a value of $D = 0.05$ cm^2 s^{-1} has been used. In the case of experiment VI, diffusion constants for the DMMP monomer and dimer were derived from reduced mobility coefficients using the Nernst–Einstein equation.[68] The findings demonstrate the validity of assumption 10.

CONCLUSIONS

Models of reactions of hydrated protons with an analyte (M) provide reaction times, ion distributions, and maximum reaction yields for a range of parameters common to APCI MS and IMS measurements. These models are sufficiently general to permit refinement or adaptation for specific conditions which may be found in various ion sources operated at or near ambient pressure in mass spectrometry. Models here disclose the sensitivity of ion distributions in time, particularly to the product $k_1[M]$, the ratio k_2/k_1, and to the introduction of hydrated protons as excess reagent. Consequently, these models may provide a foundation and tools for the development of new technologies or methodologies for ion processing in analytical measurements, based on reaction kinetics, including the separation of ion mixtures.[69]

ASSOCIATED CONTENT

Supporting Information

The Supporting Information is available free of charge at https://pubs.acs.org/doi/10.1021/jasms.1c00158.

Comments on significant figures and Figures S1–S3 (PDF)

AUTHOR INFORMATION

Corresponding Author

Elie Lattouf – *VERIFIN, Finnish Institute for Verification of the Chemical Weapons Convention, Department of Chemistry, University of Helsinki, FI-00014 Helsinki, Finland*; Email: elie.lattouf@helsinki.fi

Authors

Osmo Anttalainen – *VERIFIN, Finnish Institute for Verification of the Chemical Weapons Convention, Department of Chemistry, University of Helsinki, FI-00014 Helsinki, Finland*

Tapio Kotiaho – *Drug Research Program and Division of Pharmaceutical Chemistry and Technology, Faculty of Pharmacy, University of Helsinki, FI-00014 Helsinki, Finland; Department of Chemistry, Faculty of Science, University of Helsinki, FIN-00014 Helsinki, Finland*; orcid.org/0000-0003-0382-8578

Hanna Hakulinen – *VERIFIN, Finnish Institute for Verification of the Chemical Weapons Convention, Department of Chemistry, University of Helsinki, FI-00014 Helsinki, Finland*

Paula Vanninen – *VERIFIN, Finnish Institute for Verification of the Chemical Weapons Convention, Department of Chemistry, University of Helsinki, FI-00014 Helsinki, Finland*

Gary Eiceman – *VERIFIN, Finnish Institute for Verification of the Chemical Weapons Convention, Department of Chemistry, University of Helsinki, FI-00014 Helsinki, Finland; Department of Chemistry and Biochemistry, New Mexico State University, Las Cruces, New Mexico 88003, United States*; orcid.org/0000-0001-9026-7208

Complete contact information is available at: https://pubs.acs.org/10.1021/jasms.1c00158

Author Contributions

The authors confirm contributions to the paper as follows: modeling, programming, graphics, E.L.; assistance on computation, O.A.; data interpretation, E.L. and G.E.; manuscript preparation, E.L., T.K., and G.E.; results review, H.H. and P.V. All of the authors reviewed the results and approved the final version of the manuscript.

Notes

The authors declare no competing financial interest.

■ ACKNOWLEDGMENTS

This project, Gas Ion Distillation and Sequential Ion Processing Technologies for Identification and Visualization of Chemicals in Airborne Vapours, has received funding from the European Union's Horizon 2020 FET Open program under grant agreement no. 899261.

■ REFERENCES

(1) Horning, E. C.; Horning, M. G.; Carroll, D. I.; Dzidic, I.; Stillwell, R. N. New Picogram Detection System Based on a Mass Spectrometer with an External Ionization Source at Atmospheric Pressure. *Anal. Chem.* **1973**, *45* (6), 936−943.
(2) Tarr, M. A.; Zhu, J.; Cole, B. Atmospheric Pressure Ionization Mass Spectrometry. *Encycl. Anal. Chem.* **2000**, 1−34.
(3) Bruins, A. P. Atmospheric-Pressure-Ionization Mass Spectrometry. I. Instrumentation and Ionization Techniques. *TrAC, Trends Anal. Chem.* **1994**, *13* (1), 37−43.
(4) Bruins, A. P. Atmospheric-Pressure-Ionization Mass Spectrometry. II. Applications in Pharmacy, Biochemistry and General Chemistry. *TrAC, Trends Anal. Chem.* **1994**, *13* (2), 81−90.
(5) Proctor, C. J.; Todd, J. F. J. Alternative Reagent Ions for Plasma Chromatography. *Anal. Chem.* **1984**, *56*, 1794−1797.
(6) Eiceman, G. A. G. A.; Yuan-Feng, W.; Garcia-Gonzalez, L.; Harden, C. S. C. S.; Shoff, D. B. D. B. Enhanced Selectivity in Ion Mobility Spectrometry Analysis of Complex Mixtures by Alternate Reagent Gas Chemistry. *Anal. Chim. Acta* **1995**, *306* (1), 21−33.
(7) Monge, M. E.; Fernández, F. M. An Introduction to Ambient Ionization Mass Spectrometry. *Ambient Ion. Mass Spectr.* **2014**, No. 2, 1−22.
(8) Harris, G. a; Nyadong, L.; Fernandez, F. M. Recent Developments in Ambient Ionization Techniques for Analytical Mass Spectrometry. *Analyst* **2008**, *133* (10), 1297−1301.
(9) Shahin, M. M. Mass-Spectrometric Studies of Corona Discharges. *J. Chem. Phys.* **1966**, *45* (7), 2600−2605.
(10) Shahin, M. M. Use of Corona Discharges for the Study of Ion−Molecule Reactions. *J. Chem. Phys.* **1967**, *47* (11), 4392−4398.
(11) Fenn, J. B. Ion Formation from Charged Droplets: Roles of Geometry, Energy, and Time. *J. Am. Soc. Mass Spectrom.* **1993**, *4* (7), 524−535.
(12) Yamashita, M.; Fenn, J. B. Negative Ion Production with the Electrospray Ion Source. *J. Phys. Chem.* **1984**, *88* (20), 4671−4675.
(13) Mora, J. F. d. l.; Van Berkel, G. J.; Enke, C. G.; Cole, R. B.; Martinez-Sanchez, M.; Fenn, J. B. Electrochemical Processes in Electrospray Ionization Mass Spectrometry. *J. Mass Spectrom.* **2000**, *35* (8), 939−952.
(14) Hayen, H.; Michels, A.; Franzke, J. Dielectric Barrier Discharge Ionization for Liquid Chromatography/Mass Spectrometry. *Anal. Chem.* **2009**, *81* (24), 10239−10245.
(15) Guo, C.; Tang, F.; Chen, J.; Wang, X.; Zhang, S.; Zhang, X. Development of Dielectric-Barrier-Discharge Ionization. *Anal. Bioanal. Chem.* **2015**, *407* (9), 2345−2364.
(16) Ahrens, A.; Hitzemann, M.; Zimmermann, S. Miniaturized High-Performance Drift Tube Ion Mobility Spectrometer. *Int. J. Ion Mobility Spectrom.* **2019**, *22* (2), 77−83.
(17) Kuklya, A.; Reinecke, T.; Uteschil, F.; Kerpen, K.; Zimmermann, S.; Telgheder, U. X-Ray Ionization Differential Ion Mobility Spectrometry. *Talanta* **2017**, *162*, 159−166.
(18) Reinecke, T.; Kirk, A. T.; Heptner, A.; Niebuhr, D.; Böttger, S.; Zimmermann, S. A Compact High-Resolution X-Ray Ion Mobility Spectrometer. *Rev. Sci. Instrum.* **2016**, *87*, 053120.
(19) Turner, R. B.; Brokenshire, J. L. Hand-Held Ion Mobility Spectrometers. *TrAC, Trends Anal. Chem.* **1994**, *13* (7), 275−280.
(20) Ewing, R. G.; Atkinson, D. A.; Eiceman, G. A.; Ewing, G. J. A Critical Review of Ion Mobility Spectrometry for the Detection of Explosives and Explosive Related Compounds. *Talanta* **2001**, *54* (3), 515−529.
(21) Koyano, I. Ion−Molecule Reactions. In *Comprehensive Chemical Kinetics: Selected Elementary Reactions*; Bamford, C. H., Tipper, C. F. H., Eds.; Elsevier, 1976; Vol. *18*, pp 293−428.
(22) Munson, M. S. B.; Field, F. H. Physical and Inorganic Chemistry. *J. Am. Chem. Soc.* **1966**, *88* (12), 2621−2630.
(23) Munson, M. S. B.; Field, F. H. Chemical Ionization Mass Spectrometry. I. General Introduction. *J. Am. Chem. Soc.* **1966**, *88* (12), 2621−2630.
(24) Munson, B. Chemical Ionization Mass Spectrometry: Theory and Applications. *Encycl. Anal. Chem.* **2000**, 1−22.
(25) Chen, E. C. M.; Wentworth, W. E.; Desai, E.; Batten, C. F. Importance of Kinetics and Thermodynamics to the Electron-Capture Detector. *J. Chromatogr. A* **1987**, *399* (C), 121−137.
(26) Wentworth, W. E.; Becker, R. S. Potential Method for the Determination of Electron Affinities of Molecules: Application to Some Aromatic Hydrocarbons. *J. Am. Chem. Soc.* **1962**, *84* (22), 4263−4266.
(27) Poole, C. F. Ionization-Based Detectors for Gas Chromatography. *J. Chromatogr. A* **2015**, *1421*, 137−153.
(28) Fujii, T. *Ion/Molecule Attachment Reactions: Mass Spectrometry* **2015**, 1.
(29) Ewing, R. G.; Eiceman, G. A.; Stone, J. A. Proton-Bound Cluster Ions in Ion Mobility Spectrometry. *Int. J. Mass Spectrom.* **1999**, *193* (1), 57−68.
(30) Jurado-Campos, N.; Garrido-Delgado, R.; Martinez-Haya, B.; Eiceman, G. A.; Arce, L. Stabilities of Proton-Bound Clusters of Alkyl Alcohols, Aldehydes and Ketones in Ion Mobility Spectrometry. *Talanta* **2018**, *185*, 299−308.
(31) Allers, M.; Kirk, A. T.; Schaefer, C.; Schlottmann, F.; Zimmermann, S. Formation of Positive Product Ions from Substances with Low Proton Affinity in High Kinetic Energy Ion Mobility Spectrometry (HiKE-IMS). *Rapid Commun. Mass Spectrom.* **2021**, *35*, 1−13.
(32) Puton, J.; Nousiainen, M.; Sillanpää, M. Ion Mobility Spectrometers with Doped Gases. *Talanta* **2008**, *76* (5), 978−987.
(33) Hill, C. a; Thomas, C. L. P. A Pulsed Corona Discharge Switchable High Resolution Ion Mobility Spectrometer-Mass Spectrometer. *Analyst* **2003**, *128* (1), 55−60.
(34) McMahon, T. B. High Pressure Mass Spectrometry. In *Energetics of Stable Molecules and Reactive Intermediates*; Minas da Piedade, M. E., Ed.; Kluwer Academic Press, 1999; pp 259−280.
(35) Lau, Y. K.; Ikuta, S.; Kebarle, P. Thermodynamics and Kinetics of the Gas-Phase Reactions: H3O+(H2O)N−1 + H2O = H3O+(H2O)N. *J. Am. Chem. Soc.* **1982**, *104* (6), 1462−1469.
(36) Sunner, J.; Nicol, G.; Kebarle, P. Factors Determining Relative Sensitivity of Analytes in Positive. *Anal. Chem.* **1988**, *60*, 1300−1307.
(37) Sunner, J.; Nicol, G.; Kebarle, P. Factors Determining Relative Sensitivity of Analytes in Positive Mode Atmospheric Pressure Ionization Mass Spectrometry. *Anal. Chem.* **1988**, *60* (13), 1300−1307.
(38) Nicol, G.; Sunner, J.; Kebarle, P. Kinetics and Thermodynamics of Protonation Reactions: H3O+ (H2O)h + B = BH+ (H2O)b + (h - b + 1) H2O, Where B Is a Nitrogen, Oxygen or Carbon Base. *Int. J. Mass Spectrom. Ion Processes* **1988**, *84* (1−2), 135−155.
(39) Mautner, M. The Ionic Hydrogen Bond and Ion Solvation. 1. NH+···O, NH+···N, and OH+···O Bonds. Correlations with Proton Affinity. Deviations Due to Structural Effects. *J. Am. Chem. Soc.* **1984**, *106* (5), 1257−1264.
(40) Meot-Ner, M.; Sieck, L. W. The Ionic Hydrogen Bond. 1. Sterically Hindered Bonds. Solvation and Clustering of Protonated Amines and Pyridines. *J. Am. Chem. Soc.* **1983**, *105* (10), 2956−2961.
(41) Mackay, G. I.; Tanner, S. D.; Hopkinson, A. C.; Bohme, D. K. Gas-Phase Proton-Transfer Reactions of the Hydronium Ion at 298 K. *Can. J. Chem.* **1979**, *57* (12), 1518−1523.
(42) Bohme, D. K.; Mackay, G. I.; Tanner, S. D. An Experimental Study of the Gas Phase Kinetics of Reactions with Hydrated H3O+ Ions (N = 1−3) at 298K. *J. Am. Chem. Soc.* **1979**, *101* (14), 3724−3730.

https://doi.org/10.1021/jasms.1c00158
J. Am. Soc. Mass Spectrom. 2021, 32, 2218−2226

(43) Bohme, D. K.; Ferreira, M. A. A. Gas Phase Studies of the Influence of Solvation on Ion Reactivity. *Ionic Process. Gas Phase* **1984**, 111.
(44) Zhao, J.; Zhang, R. Proton Transfer Reaction Rate Constants between Hydronium Ion (H3O+) and Volatile Organic Compounds. *Atmos. Environ.* **2004**, *38* (14), 2177−2185.
(45) Herron, J. T.; Green, D. S. Chemical Kinetics Database and Predictive Schemes for Nonthermal Humid Air Plasma Chemistry. Part II. Neutral Species Reactions. *Plasma Chem. Plasma Process.* **2001**, *21* (3), 459−481.
(46) Yang, X.; Castleman, A. W. Temperature and Cluster Size Dependence Studies of Reactions of Protonated Water Clusters with Acetonitrile. *J. Chem. Phys.* **1991**, *95* (1), 130−134.
(47) Yang, X.; Zhang, X.; Castleman, A. W. Kinetics and Mechanism Studies of Large Protonated Water Clusters, H+(H2O)n, n = 1−60, at Thermal Energy. *Int. J. Mass Spectrom. Ion Processes* **1991**, *109* (C), 339−354.
(48) Kawai, Y.; Yamaguchi, S.; Okada, Y.; Takeuchi, K. Reactions of Protonated Water Clusters H+(H2O)n (N = 2 and 4) with D2O, Acetonitrile, Acetone, DMS, DMSO, and Pyridine. *J. Mass Spectrom. Soc. Jpn.* **2004**, *52* (5), 271−276.
(49) Viggiano, A. A.; Dale, F.; Paulson, J. F. Proton Transfer Reactions of H+(H2O)N = 2−11 with Methanol, Ammonia, Pyridine, Acetonitrile, and Acetone. *J. Chem. Phys.* **1988**, *88* (4), 2469−2477.
(50) Jazan, E.; Tabrizchi, M. Kinetic Study of Proton-Bound Dimer Formation Using Ion Mobility Spectrometry. *Chem. Phys.* **2009**, *355* (1), 37−42.
(51) Andrade, F. J.; Shelley, J. T.; Wetzel, W. C.; Webb, M. R.; Gamez, G.; Ray, S. J.; Hieftje, G. M. Atmospheric Pressure Chemical Ionization Source. 1. Ionization of Compounds in the Gas Phase. *Anal. Chem.* **2008**, *80* (8), 2646−2653.
(52) Matuszak, K. P. *The Characterization of Atmospheric Pressure Ionization/Tandem Mass Spectrometry for Direct Atmospherc Analysis*. Ph.D dissertation; University of Florida, 1988.
(53) Heptner, A.; Angerstein, N.; Reinecke, T.; Bunert, E.; Kirk, A. T.; Niedzwiecki, I.; Zimmermann, S. Improving the Analytical Performance of Ion Mobility Spectrometer Using a Non-Radioactive Electron Source. *Int. J. Ion Mobility Spectrom.* **2016**, *19* (4), 175−182.
(54) Siegel, M. W. Atmospheric Pressure Ionization. In *Plasma Chromatograph*; Carr, T. W., Ed.; Plenum Press: New York, 1984; pp 96−113.
(55) Ketkar, S. N.; Penn, S. M.; Fite, W. L. Influence of Coexisting Analytes in Atmospheric Pressure Ionization Mass Spectrometry. *Anal. Chem.* **1991**, *63* (9), 924−925.
(56) Heptner, A.; Cochems, P.; Langejuergen, J.; Gunzer, F.; Zimmermann, S. Investigation of Ion-Ion-Recombination at Atmospheric Pressure with a Pulsed Electron Gun. *Analyst* **2012**, *137* (21), 5105−5112.
(57) Goeringer, D. E. Factors Influencing the Analytical Performance of an Atmospheric Sampling Glow Discharge Ionization Source as Revealed via Ionization Dynamics Modeling. *J. Am. Soc. Mass Spectrom.* **2003**, *14* (11), 1315−1326.
(58) Sunner, J.; Ikonomou, M. G.; Kebarle, P. Sensitivity Enhancements Obtained at High Temperatures in Atmospheric Pressure Ionization Mass Spectrometry. *Anal. Chem.* **1988**, *60* (13), 1308−1313.
(59) Safaei, Z.; Eiceman, G. A. A.; Puton, J.; Stone, J. A. A.; Nasirikheirabadi, M.; Anttalainen, O.; Sillanpää, M. Differential Mobility Spectrometry of Ketones in Air at Extreme Levels of Moisture. *Sci. Rep.* **2019**, *9* (1), 5593.
(60) Safaei, Z.; Willy, T. J.; Eiceman, G. A.; Stone, J. A.; Sillanpää, M. Quantitative Response in Ion Mobility Spectrometry with Atmospheric Pressure Chemical Ionization in Positive Polarity as a Function of Moisture and Temperature. *Anal. Chim. Acta* **2019**, *1092*, 144−150.
(61) Ewing, R. G.; Atkinson, D. A.; Clowers, B. H. Direct Real-Time Detection of RDX Vapors under Ambient Conditions. *Anal. Chem.* **2013**, *85* (1), 389−397.
(62) Scott, a. D.; Hunter, E. J.; Ketkar, S. N. Use of a Clustering Reaction To Detect Low Levels of Moisture in Bulk Oxygen Using an Atmospheric Pressure Ionization Mass Spectrometer. *Anal. Chem.* **1998**, *70* (9), 1802−1804.
(63) Bohme, D. K.; Mackay, G. I.; Tanner, S. D. An Experimental Study of the Gas-Phase Kinetics of Reactions with Hydrated H3O +Ions(n = 1−3) at 298 K. *J. Am. Chem. Soc.* **1979**, *101* (14), 3724−3730.
(64) Tolmachev, A. V. A.; Clowers, B. H. B.; Belov, M. E.; Smith, R. D. Coulombic Effects in Ion Mobility Spectrometry. *Anal. Chem.* **2009**, *81* (12), 4778−4787.
(65) Jasper, A. W.; Pelzer, K. M.; Miller, J. A.; Kamarchik, E.; Harding, L. B.; Klippenstein, S. J. Predictive a Priori Pressure-Dependent Kinetics. *Science (Washington, DC, U. S.)* **2014**, *346* (6214), 1212−1215.
(66) Ilbeigi, V.; Tabrizchi, M. Peak-Peak Repulsion in Ion Mobility Spectrometry. *Anal. Chem.* **2012**, *84* (8), 3669−3675.
(67) Sunner, J.; Nicol, G.; Kebarle, P. Factors Determining Relative Sensitivity of Analytes in Positive Mode Atmospheric Pressure Ionization Mass Spectrometry. *Anal. Chem.* **1988**, *60* (13), 1300−1307.
(68) Anttalainen, O.; Lattouf, E.; Kotiaho, T.; Eiceman, G. A. Ion Density of Positive and Negative Ions at Ambient Pressure in Air at 12 to 136 Mm from 4.9 KV Soft X-Ray Source. *Rev. Sci. Instrum.* **2021**, *92*, 054104.
(69) Ito, T.; Namiki, N.; Lee, M.; Emi, H.; Otani, Y. Electrostatic Separation of Volatile Organic Compounds by Ionization. *Environ. Sci. Technol.* **2002**, *36* (19), 4170−4174.

https://doi.org/10.1021/jasms.1c00158
J. Am. Soc. Mass Spectrom. 2021, 32, 2218−2226